# A Modular Three-Dimensional Bioprinter for Printing Porous Scaffolds for Tissue Engineering

**Linnea Warburton**[1]
Department of Mechanical Engineering,
University of California at Berkeley,
Berkeley, CA 94709
e-mail: linneawarburton@berkeley.edu

**Leo Lou**
Department of Bioengineering,
University of California at Berkeley,
Berkeley, CA 94709

**Boris Rubinsky**
Department of Mechanical Engineering,
University of California at Berkeley,
Berkeley, CA 94709;
Department of Bioengineering,
University of California at Berkeley,
Berkeley, CA 94709

*Three-dimensional (3D) bioprinting is a fabrication method with many biomedical applications, particularly within tissue engineering. The use of freezing during 3D bioprinting, aka "3D cryoprinting," can be utilized to create micopores within tissue-engineered scaffolds to enhance cell proliferation. When used with alginate bio-inks, this type of 3D cryoprinting requires three steps: 3D printing, crosslinking, and freezing. This study investigated the influence of crosslinking order and cooling rate on the microstructure and mechanical properties of sodium alginate scaffolds. We designed and built a novel modular 3D printer in order to study the effects of these steps separately and to address many of the manufacturing issues associated with 3D cryoprinting. With the modular 3D printer, 3D printing, crosslinking, and freezing were conducted on separate modules yet remain part of a continuous manufacturing process. Crosslinking before the freezing step produced highly interconnected and directional pores, which are ideal for promoting cell growth. By controlling the cooling rate, it was possible to produce pores with diameters from a range of 5 μm to 40 μm. Tensile and firmness testing found that the use of freezing does not decrease the tensile strength of the printed objects, though there was a significant loss in firmness for strands with larger pores.* [DOI: 10.1115/1.4053198]

## 1 Introduction

Three-dimensional (3D) bioprinting, aka the 3D printing of biomaterials, is a fabrication method with applications from tissue engineering to medical device research, to food technology. 3D bioprinting allows for the precise and controlled deposition of biomaterials to produce objects with complex architecture [1]. For tissue engineering, 3D printed hydrogel scaffolds provide the physical space and mechanical support for new tissue to develop until the scaffold is eventually absorbed by the body [2, 3]. One category of 3D bioprinting is "3D cryoprinting," in which the printed material is frozen during the 3D printing process. Previously, 3D cryoprinting has been used to print scaffolds for bone tumor defects as well as to replicate the softest tissues of the human body [4,5]. 3D cryoprinting offers several unique advantages. First, freezing the object as it is 3D printed increases its rigidity, facilitating the manufacturing of complex structures from an ink that is usually soft at deposition [5,6]. Second, freezing cell-laden bio-inks at optimal cooling rates during deposition can preserve the cells, preventing them from succumbing to environmental stressors during the printing process. Third, 3D cryoprinting can streamline the manufacturing process, as many biotechnological applications require the product to be first printed and then frozen for preservation and transportation and thawed for use. Another potential advantage of freezing during printing is that microscale pores are created by the ice crystal growth in the printed object. Tissue-engineered scaffolds must be highly porous for cell seeding and ingrowth, with typical porosities above 90% [7]. In fact, 3D bioprinting is often chosen as a fabrication method for tissue-engineered scaffolds because of its ability to precisely print macropores on the scale of 1 mm. Thus, 3D bioprinting coupled with freezing can be used to create complex structures with both controlled macropores and micropores for cell growth.

In the various methods of 3D cryoprinting, the process of freezing occurs along the temperature gradient, on a specific axis. When freezing occurs along a specified axis, this process is known as directional freezing. During directional freezing, ice crystals grow forward as a dendritic ice front, creating directional pores (see Fig. 1).

This directionality has special significance within the field of tissue engineering, as directional, interconnected pore networks within scaffolds are crucial for cell growth [8]. An interconnected pore network encourages cell attachment and vascularization, while directional pores aid directional cell growth and provide faster diffusion for drug delivery [9–11]. While directional freezing has rarely been studied in conjunction with 3D bioprinting, it has been used extensively to create directional, interconnected pores in biomaterials [9,12–16]. Notably, Bozkurt et al. used

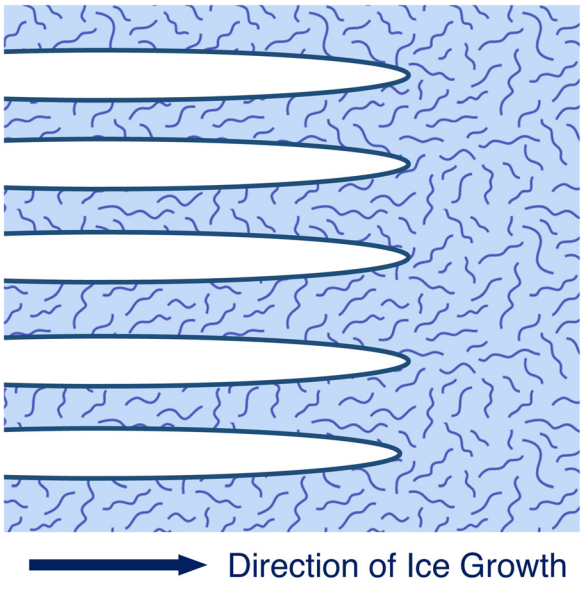


**Fig. 1 Ice crystal growth along an axis during directional freezing**

[1]Corresponding author.

Contributed by the Heat Transfer Division of ASME for publication in the Journal of Heat Transfer. Manuscript received September 13, 2021; final manuscript received November 27, 2021; published online January 18, 2022. Assoc. Editor: Ram Devireddy.

  

directional freezing to create longitudinal pores in collagen scaffolds for axonal regeneration, and Qi et al. used directional freezing to create oriented pores in alginate/calcium phosphate cement scaffolds [17,18].

This paper will address several important manufacturing issues related to 3D cryoprinting, with a focus on cryoprinting with alginates. Alginates are one of the most popular materials used as bioinks, as alginate scaffolds have been found to promote wound healing [19,20]. For alginate scaffolds to achieve the required mechanical characteristics for tissue engineering, they must be ionically crosslinked by a crosslinker such as $CaCl_2$ after printing. Crosslinking the alginate before printing results in an ink with a variable viscosity that increases in time—causing difficulties in designing the ink flow through the printing nozzle. Therefore, the alginates are often crosslinked during or after the deposition of the printed material. In 3D cryoprinting, there is another manufacturing step in addition to printing and crosslinking, which is freezing. Therefore, the order of manufacturing the 3D cryoprinted object can be either: (a) deposition, freezing, thawing, and crosslinking or (b) deposition, crosslinking, freezing, and thawing. A major goal of the freezing process in cryoprinting is to generate controlled microstructures with desired dimensions and orientation. This can be achieved through controlled cooling rates during freezing. Another important question in the design of a manufacturing process using cryoprinting is how does the freezing and the resulting microstructure affect the ultimate mechanical properties of the printed object. Porous hydrogels for tissue engineering must have high porosity while maintaining mechanical strength, or they will not survive in the body [10]. The goal of this experimental study is to evaluate how the parameters of a typical 3D cryoprinting process, including cooling rate and order of crosslinking, affect the microstructure and the mechanical properties of a 3D printed object. To study the effect of each step separately, we have designed a modular 3D printer in which the steps of printing, freezing, and crosslinking are done separately in the desired order and with the desired parameters. To facilitate breaking apart these three steps, while maintaining continuity of the manufacturing process, each step takes place on a moving stage that allows the printed object to move from one module to another. In addition to serving as a means for fundamental studies, this modular technology may also have value as an industrial means for large-scale continuous manufacturing of bio-engineering products.

Using the modular 3D printer, we investigate the influence of crosslinking and cooling rates over the shape and distribution of the pores within 3D printed sodium alginate strands. The first goal of this study was to investigate how crosslinking before or after directional freezing impacts the creation of pores. The second goal was to investigate the influence of cooling rate on the shape and size of the pores. The third goal was to evaluate whether the use of directional freezing negatively affected the mechanical properties of the sodium alginate scaffold. The tensile strength and firmness of each type of directionally frozen scaffold were tested to evaluate if the directionally frozen scaffolds would still provide sufficient mechanical support for tissue growth.

## 2 Materials and Methods

**2.1 Hydrogel Preparation.** The printing ink was prepared by dissolving 2% sodium alginate (Spectrum Chemical Mfg. Corp. Gardena, CA) into de-ionized water. A magnetic stir plate was used to mix the solution at room temperature until it became homogenous. The solution was then stored at 4 °C in a refrigerator for at least 24 h. The 2% calcium chloride ($CaCl_2$) crosslinker was prepared by dissolving 2 g of $CaCl_2$ dihydrate powder (Fisher Scientific, Fairlawn, NJ) to 100 mL of de-ionized water and mixing it with the magnetic stir plate.

**2.2 Modular Three-Dimensional Printer.** A custom modular 3D printer was designed and built for 3D printing, crosslinking, and directional freezing (see Fig. 2). Each of the three processes took place on a separate module that could be rearranged to change the order of fabrication. For example, the crosslinking module could be switched with the directional freezing module so that directional freezing occurred first, or vice versa. As stated earlier, the first goal of this study was to investigate whether crosslinking should occur before or after directional freezing. The second goal was to investigate the influence of both rapid and slow cooling rates on the shape and size of the directional pores. To investigate these variables, the alginate strands were prepared using four possible treatments. The first option was crosslinking then rapid freezing at 0.5 deg/s (CL-FR rapid). The second option was crosslinking then slow freezing at 0.02 deg/s (CL-FR slow). The third option was rapid freezing at 0.5 deg/s then crosslinking (FR-CL rapid), and the fourth option was slow freezing at 0.02 deg/s then crosslinking (FR-CL slow). In addition, control strands were fabricated by printing and then crosslinking directly after, with no use of directional freezing.

*2.2.1 3D Printing Module.* The 3D printing module consisted of syringe pump extruder printing onto a conveyor belt. The syringe pump extruder with a 60 cc syringe, and extrusion was powered by a Harvard PHD 2000 Syringe Pump (Hollington, MA). 2% sodium alginate at room temperature was pushed from the syringe through a plastic tube and down through a 12-gage metal nozzle (2.16 mm diameter). The nozzle moved back and forth on a belt along the *y*-axis, and deposited sodium alginate onto a print plate on the conveyor belt, which moved along the *x*-axis. To simplify analysis of factors affecting pore creation, single strands of sodium alginate were printed. The strands were 150 mm long and 2.5 mm wide and printed at a speed of 15 mm/second. When printing finished, the conveyor belt carried the print plate along the *x*-axis and onto the next module.

*2.2.2 Crosslinking Module.* For sodium alginate to achieve the required mechanical characteristics for tissue engineering, it must be ionically crosslinked by a crosslinker such as $CaCl_2$ after printing. The crosslinking module consisted of a conveyor belt moving along the *x*-axis and a stationary sprayer above the belt. The sprayer consisted of a custom syringe pump extruder attached to an atomizer, which sprayed a heavy mist of $CaCl_2$ droplets. As the print plate traveled down the conveyor belt, it stopped under the sprayer, and the printed object was sprayed thoroughly with 2% $Cacl_2$. The print plate remained stationary for 10 minutes as crosslinking occurred, and then the conveyor belt pulled the print plate toward the next module.

*2.2.3 Directional Freezing Module.* During the directional freezing process, the print plate was pulled at a fixed rate across a room temperature plate to a cold plate. This resulted in ice crystal growth along the x-axis, from the cold plate toward the room temperature plate. The print plate was attached to a string that was wound around a pulley and driven by a stepper motor (see Fig. 2). The cold plate was a CP3001 Wieland Microcool liquid-cooled cold plate, and either liquid nitrogen or ethylene glycol was circulated through the plate as the cooling fluid (Decatur, Al). For the rapid freezing process, liquid nitrogen was circulated through the cold plate with the surface of the plate reaching temperatures of −196 °C. For the slow freezing process, a 45% ethylene glycol and water solution was circulated through the plate by a Neslab RTE-140 cooling bath, and six CP68475H-2 Peltier elements were placed on top of the cooling plate, with a resulting surface temperature of −40 °C (Thermo Scientific, Waltham, MA, CUI Devices, Lake Oswego, OR) The temperature of the print plate in proximity to the alginate strands was measured throughout the freezing process with a K type thermocouple. The resulting cooling rate of the alginate strands for the rapid freezing process was approximately 0.5 deg/s and the cooling rate for the slow freezing process was approximately 0.02 deg/s. After completion of both the crosslinking and freezing processes, the resulting alginate strands were cut into uniform pieces for imaging and testing.

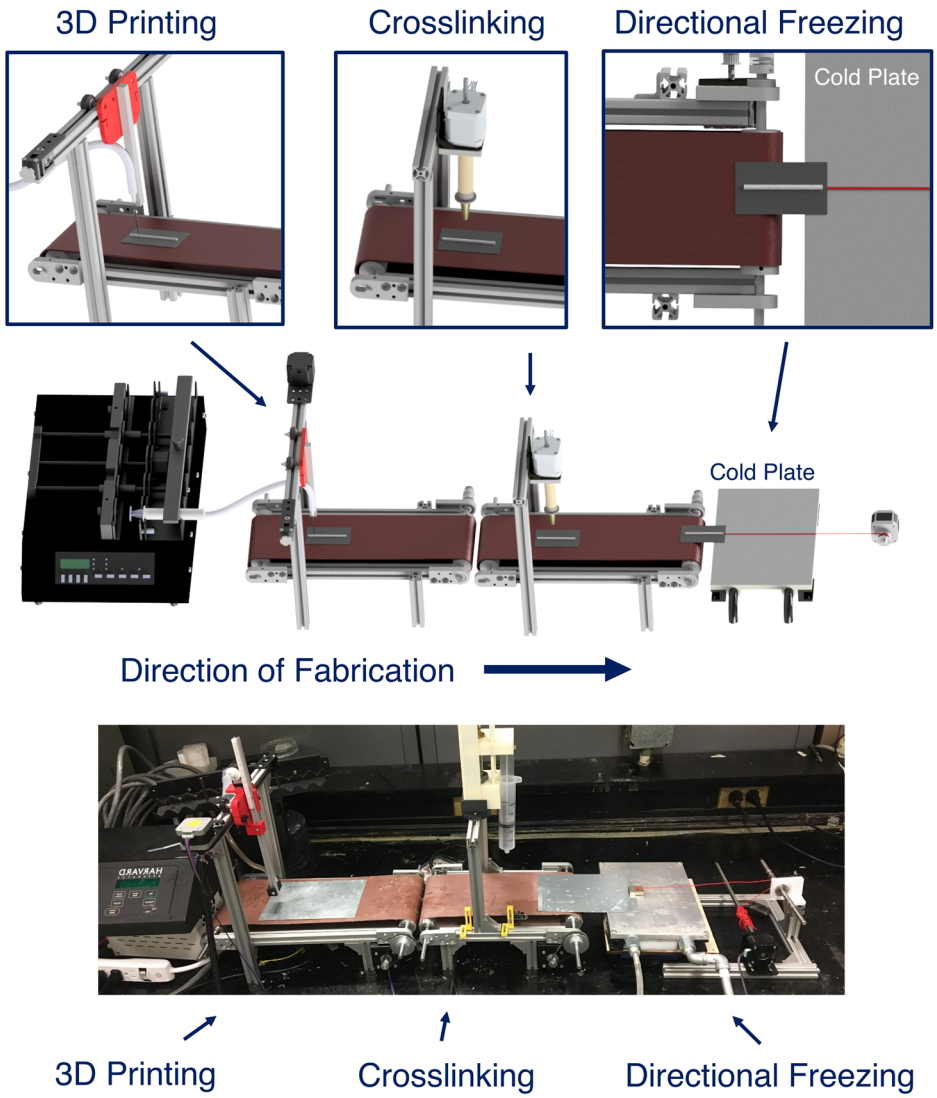


**Fig. 2 The modular 3D printer, including the 3D printing, crosslinking, and directional freezing modules. The crosslinking and directional freezing modules can be switched depending on the desired order of fabrication.**

**2.3 Surface Characterization.** Due to the transparency of the alginate strands, it was possible to view the pores under a Nikon Eclipse TE300 inverted microscope (Nikon, Tokyo, Japan). The samples were untreated before being viewed in the inverted microscope and ImageJ was used to calculate the true size of the pores (NIH, Bethesda, MD). SEM imaging was done using a Hitachi TM-4000 Scanning Electron Microscope (Hitachi, Tokyo, Japan). The samples were fixed in 2% glutaraldehyde with a 0.1 M Sodium cacodylate buffer (*p*H 7.2). After ethanol dehydration they were dried in a Tousimis Auto-Samdri 815 critical point dryer for an hour (Rockville, MD).

### 2.4 Mechanical Characterization

*2.4.1 Tensile Testing.* Uniaxial tensile testing was conducted at room temperature using an Instron® 5940 tensile testing machine (Instron, Norwood, MA). To enhance gripping during the test, the ends of the alginate strands were glued between squares of sandpaper. The hydration of the strands was maintained by storing them in a $CaCl_2$ bath up until testing. As testing temperature and testing speed affect the measured tensile properties of polymers, all samples were tested at the same temperature and testing speed. Testing was performed at a speed of 15 mm per minute, and tensile tests were conducted with ten different samples for each treatment, including a control group. The ultimate tensile strength (MPa) was defined as the peak stress on the stress–strain graph.

*2.4.2 Texture Profile Analysis.* A texture profile analysis is a type of compression test developed by the food industry to evaluate the textural properties of food. During a texture profile analysis, a probe descends at a set rate through a sample and then retracts. We evaluated the firmness and work to shear of the alginate strands using a TA-XTPlus texture analyzer (Texture Technology Corp., Scarsdale, NY) with a TA-47 Lexan blade and a 1 kg load cell. The strands were oriented perpendicular to the TA-47 blade on a Lexan base. The blade descended through the strands at 1 mm/s until it touched the base, reached a threshold force, and retracted to finish the test. Tests were performed at room temperature and the samples were submerged in a $CaCl_2$ bath until testing to maintain hydration. Seven strands were tested for each treatment and each strand was tested in three different places. Firmness (N), which is also referred to as hardness or deformation force in the literature, corresponded to the maximum force noted in the force/time graph. The work required to shear the sample (N*m) corresponded to the area under the curve.

*2.4.3 Statistical Analysis.* Comparison between means was made using a student's *T*-test with a significance level set at

$p < 0.05$. Data points more than two standard deviations from the mean were removed.

## 3 Results and Discussion

*3.1.1 Surface Characterization.* Directional pores were visible in the CL-FR Rapid, CL-FR slow, and FR-CL slow strands, with pores in the CL-FR rapid and CL-FR slow strands showing high interconnectivity. Pores in the FR-CL rapid strands were not visible under the inverted microscope, but SEM images of cross section revealed that pores existed. It is possible that freezing process altered the surface of the FR-CL strand, making it opaque and preventing the pores from being visible under the inverted microscope. As expected, no pores were visible in the control strands (Fig. 3).

The visible pores created by directional freezing ranged from a 5 $\mu$m diameter in the CL-FR rapid strands to 40 $\mu$m diameter in the CL-FR slow pores. This difference in size between the pores in the slow cooled and rapid cooled strands is consistent with theory and results from the literature. High freezing temperatures and a long time for crystallization produce large ice crystals, while low freezing temperatures and a quick time for crystallization produces smaller, finer crystals [13,21]. Malecki et al. and Nishihara et al. used directional freezing in gels and found that larger pores were produced by a low cooling temperature and low cooling rate [9,15]. The observed pores were on the proper scale for cell growth [22]. According to tissue regeneration studies, 5 $\mu$m is an optimal pore size for neovascularization 5–15 $\mu$m is optimal for fibroblast ingrowth, 20–125 $\mu$m is optimal for adult skin, 100–350 $\mu$m is optimal for bone regeneration, and 40–100 $\mu$m is optimal for osteoid ingrowth [23]. Thus, by controlling the cooling rate, different size pores can be created for different types of cell growth. Larger pores could likely be created by further slowly the cooling rate, and macropores can be created using the 3D printing process.

An interesting phenomenon observed here was the difference in ice crystal pattern between the CL-FR and the FR-CL strands. The CL-FR strands displayed highly interconnected pores, while in contrast, the FR-CL slow strands displayed dendritic pores with long columnar primary dendrites and evenly spaced secondary dendrites. Faster cooling rates are expected to produce smooth primary dendrite arms that are spaced quite close together and have relatively little secondary dendrite growth, while slow cooling rates are expected to produce primary dendrite arms that are farther apart and have more secondary dendrite growth [4]. Interestingly, this effect is seen in the FR-CL slow pores but not in the CL-FR slow pores. Ultimately, the highly interconnected pores viewed in the CL-FR strands are preferable for cell growth over the more parallel, spaced-out pores viewed in the FR-CL slow strands.

*3.2.1 Tensile Testing.* If 3D printed scaffolds for tissue engineering do not have enough mechanical strength to maintain their shape during cell proliferation, the emerging tissue will be deformed [24]. Porosity and pore size greatly affect the mechanical properties of porous hydrogels, so it is critical to evaluate if these hydrogels have sufficient mechanical strength [24]. Here, we used uniaxial tensile testing to compare control strands with strands that have undergone various types of directional freezing.

As reported in Table 1, all strands had an ultimate tensile strength above 0.16 MPa, and the ultimate tensile strength of the CL-FR rapid, CL-FR slow, and FR-CL rapid strands was higher than the control strands (see Fig. 4). A student's *t*-test found that the increase in tensile strength between the CL-FR rapid and the control strands was statistically significant, but the other treatments were not significantly different from the control strands. Thus, we can conclude that the use of directional freezing will not

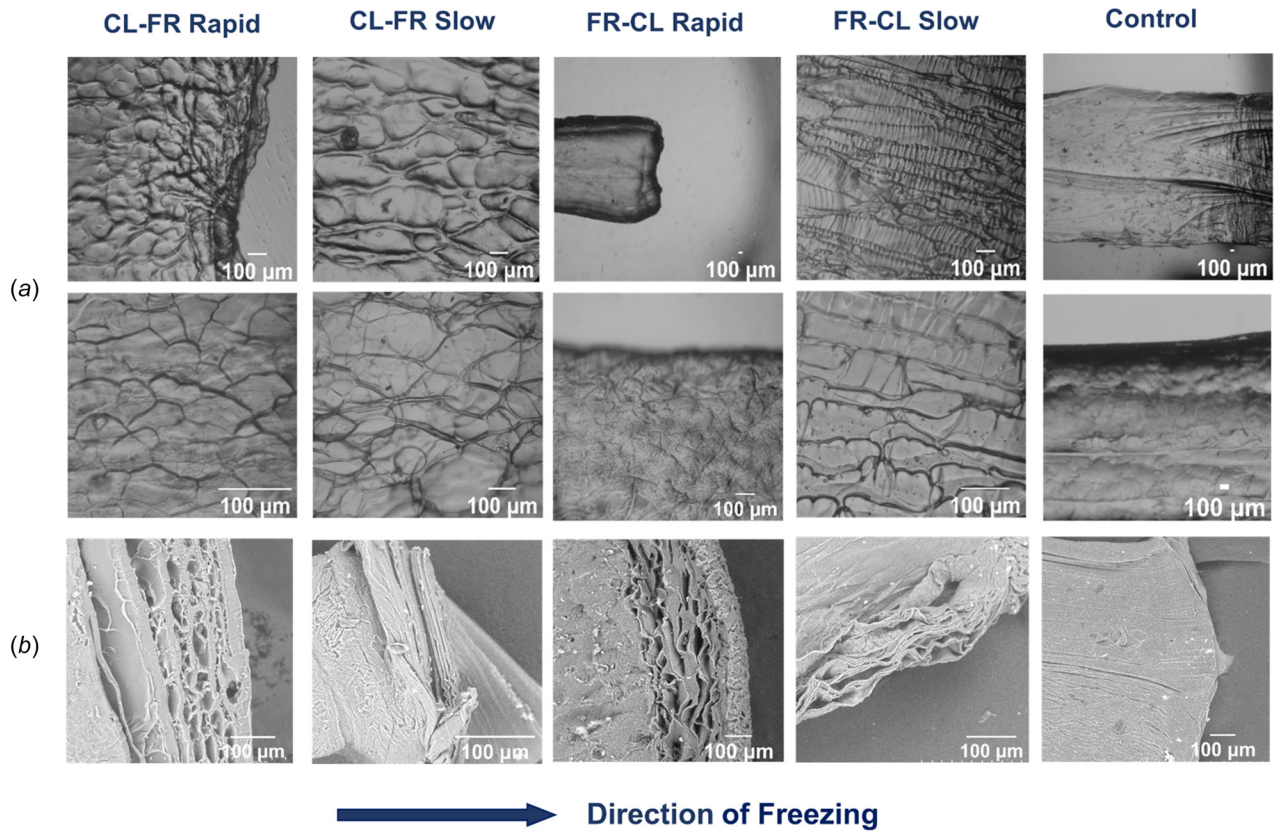


**Fig. 3 (*a*) Inverted microscope images of the alginate strands taken from a top view and (*b*) SEM images of cross section of the alginate strands**

**Table 1 Mean and standard deviations from tensile testing**

| Treatment | Tensile strength (MPa) |
|---|---|
| Control | 0.204 ± 0.047 |
| CL-FR rapid | 0.292 ± 0.069 |
| CL-FR slow | 0.237 ± 0.082 |
| FR-CL rapid | 0.260 ± 0.074 |
| FR-CL slow | 0.168 ± 0.059 |

decrease the tensile strength of a sodium alginate scaffold as to prevent it from being usable in the body. In fact, some directional freezing treatments can marginally increase the tensile strength of a sample. It is possible that the increase in strength in the CL-FR rapid strands is due to the directionality of the pores. Liu et al. found that directionally freeze-thawed (graphene oxide (GO)/polyvinyl alcohol (PVA)) hydrogels had a higher tensile strength than freeze-thawed GO-PVA hydrogels and theorized that the increase in strength was due to the organized network of hydrogel created by directional freezing [25]. The range of tensile strengths measured here is also consistent with the tensile strength of 2% sodium alginate that is reported in the literature, although different testing speeds were used. Fu et al. tested six grades and ten batches of 2% sodium alginate and found ultimate tensile strengths between 0.123 MPa and 0.679 MPa [26].

It is important to note that the tensile strength of 2% sodium alginate strands is significantly less than the tensile strength of normal human skin, which has an ultimate tensile strength of 7.7 MPa [24]. There are various ways of modifying sodium alginate to achieve tensile strengths that are closer to human tissue. For example, the addition of materials such as graphene oxide or poly lactic- coglycolic acid can increase the mechanical strength of alginate scaffolds [18,27]. Submerging samples in a bath of crosslinker for an extended time period, such as for two weeks, can also improve mechanical strength [28]. While the alginate strands prepared here have a tensile strength that is significantly lower than human skin, ultimately the tissue-engineered scaffold

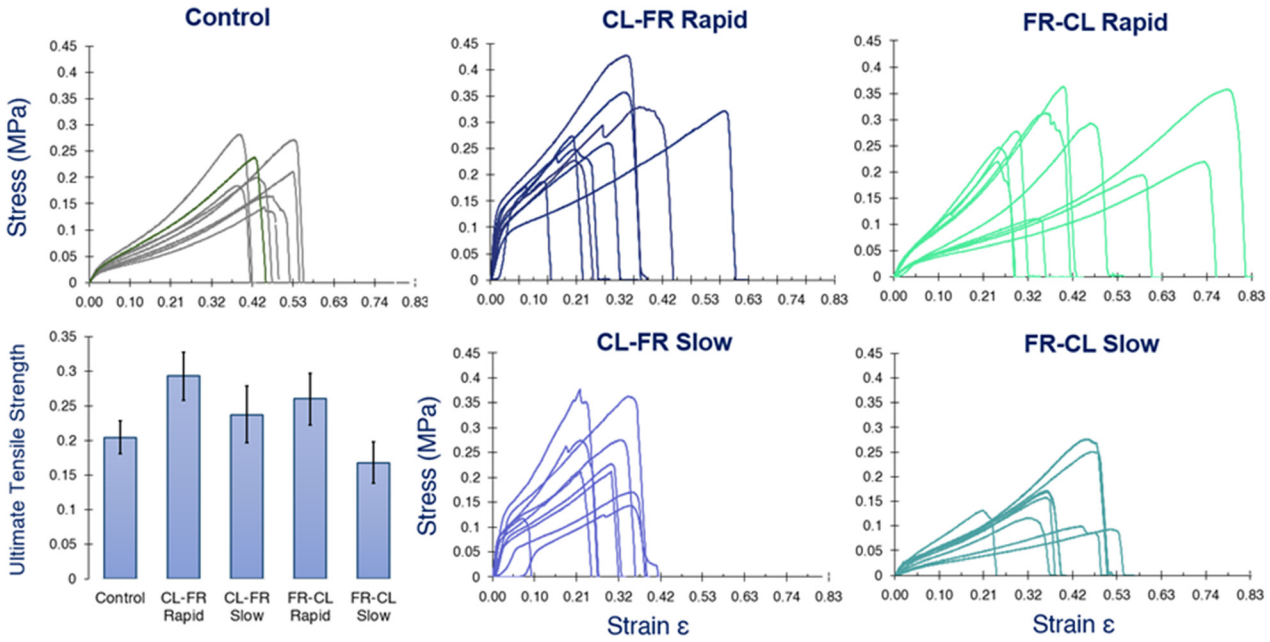


**Fig. 4 (*a*) Stress–strain curves for control strands, CL-FR rapid, FR-CL rapid, CL-FR slow, and FR-CL slow treatments. Tensile testing was conducted on ten samples for each treatment. (*b*) Average ultimate tensile strengths of all treatments. Treatments in group a) are statistically significant difference from the Control strands while treatments labeled in group b) are statistically significant difference. Error bars represent ± one standard deviation from the mean.**

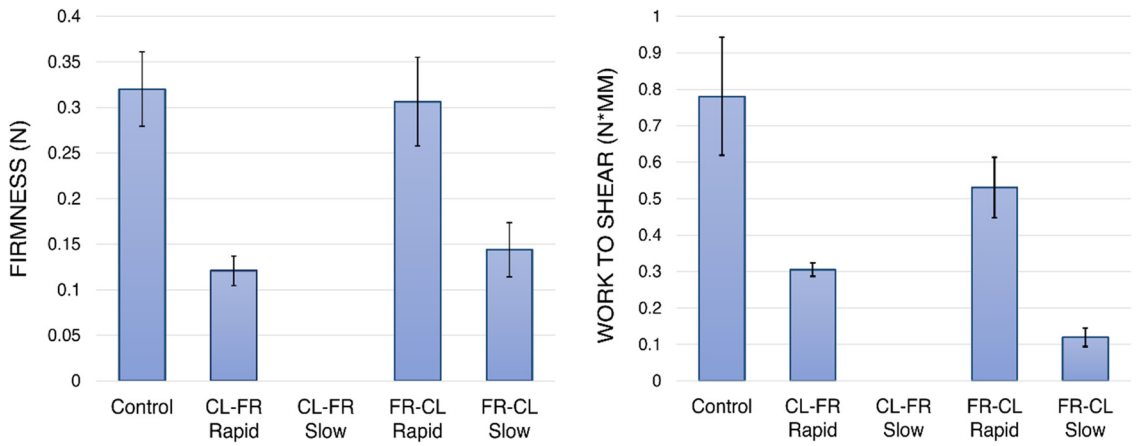


**Fig. 5 Bar graphs for firmness and work to shear. Error bars represent ± one standard deviation from the mean.**

**Table 2 Means and standard deviations for firmness and work to shear**

| Treatment | Firmness (N) | Work to shear sample (N*m) |
|---|---|---|
| Control | 0.320 ± 0.082 | 0.780 ± 0.323 |
| CL-FR rapid | 0.121 ± 0.033 | 0.305 ± 0.037 |
| CL-FR slow | NA | NA |
| FR-CL rapid | 0.272 ± 0.056 | 0.531 ± 0.165 |
| FR-CL slow | 0.144 ± 0.059 | 0.120 ± 0.051 |

is not intended to act as a permanent replacement for native tissue. Rather, it is needed to withstand temporary expansive and contractive forces in a wound or during cell growth [24].

*3.2.2 Texture Profile Analysis.* A texture profile analysis was used to evaluate the extent to which directional freezing treatments altered the mechanical properties of the sodium alginate strands. Previously, Hurler et al., proposed the use of texture profile analysis as a fast and reproducible method of characterizing hydrogels and determining their potential for wound therapy [29]. A sample's firmness and work to shear represent its resistance to deformation in the body [29] (Fig. 5 and Table 2).

Unlike the tensile strength of the samples, which increased with the addition of a directional freezing process, directional freezing decreased the firmness of alginate strands. This is not unexpected, as increases in the porosity of hydrogels typically decrease the hydrogel's mechanical strength [23]. The CL-FR Slow strands had such a loss in firmness that they could not be tested with the TA-XTPlus texture analyzer. Thus, while CL-FR Slow displayed large and highly interconnected pores, the loss in mechanical strength may prevent this treatment from producing useful tissue-engineered scaffolds. The firmness and work to shear of CL-FR Rapid and FR-CL Slow were significantly lower than the control strands; however, there was not a statistically significant difference between the FR-CL Rapid strands and the control strands. Likely, the loss of firmness in the slow-frozen strands is due to the larger pores that were created through the slow freezing process. If so, this suggests that the FR-CL strands have a lower porosity than the CL-FR strands, which is suggested as well by the tensile data and the microscope images. As with the tensile data, there is a statistically significant difference between the CL-FR and FR-CL treatments, which suggests that these two methods create different pore patterns.

## 4 Conclusion

As 3D bioprinting becomes a more popular method of fabrication, it is important to explore manufacturing methods that can achieve complex design goals. In this study, we used a novel modular 3D printer to print, crosslink, and directionally freeze hydrogel strands for tissue engineering. By separating these processes onto three modules, we created a manufacturing system where the order of fabrication can be altered, and each process could take place using unique parameters. This modular technology not only aids fundamental studies but may also be valuable for the large-scale continuous manufacturing of biomaterials. The use of directional freezing coupled with 3D bioprinting created directional pores with diameters from 5 $\mu$m to 40 $\mu$m. Our first goal was to investigate how crosslinking before or after directional freezing impacted the creation of pores. Hydrogel strands that were crosslinked before undergoing directional freezing showed pore patterns with greater interconnectivity, while strands that were crosslinked after directional freezing displayed spaced out pores with less interconnectivity. Our second goal was to investigate the influence of both rapid and slow cooling rates on the size of the pores. As expected based on previous results, faster cooling rates resulted in smaller pores on the scale of 5 $\mu$m, and slower cooling rates resulted in larger pores on the scale of 40 $\mu$m. Thus, by altering parameters such as crosslinking and cooling rate, it is possible to control the pattern and size of the micropores. Our third goal was to evaluate the mechanical properties of the directionally frozen scaffolds and determine if they would still provide sufficient support for tissue growth. The directionally frozen strands had similar tensile strengths to the control strands and values reported in the literature. The strands which were crosslinked and then rapidly frozen had a higher tensile strength than the control strands, possibly due to the directional pores. The results from the texture profile analysis found that directionally freezing the scaffolds decreased their firmness and work to shear. In the case of strands that were crosslinked and slowly frozen, the loss in firmness and work to shear was significant, likely due to the large size of the pores. Further work with the modular 3D printer should evaluate scaffolds printed with cell-laden bio-inks. Due to the modular nature of the printer, it will be possible to assess cell viability during each stage of the manufacturing process and to then tune parameters at each stage to avoid cell death. Additionally, to simplify analysis of the effects of various parameters on pore creation, only single strands of sodium alginate were 3D printed in this study. However, in future research the abilities of 3D printing can be further utilized to create to create customized pore morphologies, complex shapes, and multimaterial structures [9]. In combination with directional freezing, 3D printing can thus be used to create complicated structures with both a macrostructure and a microstructure.


## Acknowledgment

Funding is gratefully acknowledged from the NSF Engineering Research Center for Advanced Technologies for Preservation of Biological Systems (ATP-Bio) NSF EEC #1941543. L.W. was supported by the National Science Foundation Graduate Research Fellowship Program. Special thanks to Gabriel Lopez (UC Berkeley) for aiding in the tensile testing and to Cristina Bilbao-Sainz (USDA) for aiding with the texture profile analysis.

## Funding Data

- NSF Engineering Research Center for Advanced Technologies for Preservation of Biological Systems (ATP-Bio) NSF EEC (Grant No. 1941543; Funder ID: 10.13039/100000001).


## References


[1] Vijayavenkataraman, S., Yan, W. C., Lu, W. F., Wang, C. H., and Fuh, J. Y. H., 2018, "3D Bioprinting of Tissues and Organs for Regenerative Medicine," Adv. Drug Deliv. Rev., **132**, pp. 296–332.

[2] Irvine, D. J., Stachowiak, A. N., and Hori, Y., 2008, "Lymphoid Tissue Engineering: Invoking Lymphoid Tissue Neogenesis in Immunotherapy and Models of Immunity," Semin. Immunol., **20**(2), pp. 137–146.

[3] Sun, J., and Tan, H., 2013, "Alginate-Based Biomaterials for Regenerative Medicine Applications," Materials, **6**(4), pp. 1285–1309.

[4] Wang, C., Ye, X., Zhao, Y., Bai, L., He, Z., Tong, Q., Xie, X., Zhu, H., Cai, D., Zhou, Y., Lu, B., Wei, Y., Mei, L., Xie, D., and Wang, M., 2020, "Cryogenic 3D Printing of Porous Scaffolds for in Situ Delivery of 2D Black Phosphorus Nanosheets, Doxorubicin Hydrochloride and Osteogenic Peptide for Treating Tumor Resection-Induced Bone Defects," Biofabrication, **12**(3), p. 035004.

[5] Tan, Z., Parisi, C., Di Silvio, L., Dini, D., and Forte, A. E., 2017, "Cryogenic 3D Printing of Super Soft Hydrogels," Sci. Rep., **7**(1), p. 16293.

[6] Warburton, L., Liu, C., Dharmadhikari, K., Vemulakonda, P., Cheema, Y., Kewelramani, N., and Sidelnikov, D.,et al 2019, "Utilization of Cryogenic Temperatures to Reduce Line Width Variability in 3D Bioprinted Hydrogel Lattices," Trans. Addit. Manuf. Meets Med., **1**(1), epub.

[7] Freyman, T. M., Yannas, I. V., and Gibson, L. J., 2001, "Cellular Materials as Porous Scaffolds for Tissue Engineering," Prog. Mater. Sci., **46**(3–4), pp. 273–282.

[8] Feng, P., Wei, P., Shuai, C., and Peng, S., 2014, "Characterization of Mechanical and Biological Properties of 3-D Scaffolds Reinforced With Zinc Oxide for Bone Tissue Engineering," PLoS One, **9**(1), p. e87755.

[9] Maleki, H., Shahbazi, M. A., Montes, S., Hosseini, S. H., Eskandari, M. R., Zaunschirm, S., Verwanger, T., Mathur, S., Milow, B., Krammer, B., and Hüsing, N., 2019, "Mechanically Strong Silica-Silk Fibroin Bioaerogel: A Hybrid Scaffold With Ordered Honeycomb Micromorphology and Multiscale Porosity for Bone Regeneration," ACS Appl. Mater. Interfaces, **11**(19), pp. 17256–17269.

[10] Tetik, H., Wang, Y., Sun, X., Cao, D., Shah, N., Zhu, H., Qian, F., and Lin, D., 2021, "Additive Manufacturing of 3D Aerogels and Porous Scaffolds: A Review," Adv. Funct. Mater., **2103410**, p. 2103410.
[11] De France, K. J., Xu, F., and Hoare, T., 2018, "Structured Macroporous Hydrogels: Progress, Challenges, and Opportunities," Adv. Healthcare Mater., **7**(1), pp. 1–17.
[12] Preciado, J. A., Cohen, S., Skandakumaran, P., and Rubinsky, B., 2003, "Utilization of Directional Freezing for the Construction of Tissue Engineering Scaffolds," Am. Soc. Mech. Eng. Heat Transfer Div., **374**(4), pp. 439–442.
[13] Zhang, Y., Wang, C., Fu, L., Ye, S., Wang, M., and Zhou, Y., 2019, "Fabrication and Application of Novel Porous Scaffold in Situ-Loaded Graphene Oxide and Osteogenic Peptide by Cryogenic 3D Printing for Repairing Critical-Sized Bone Defect," Molecules, **24**(9), p. 1669.
[14] Gutiérrez, M. C., Ferrer, M. L., and del Monte, F., 2008, "Ice-Templated Materials: Sophisticated Structures Exhibiting Enhanced Functionalities Obtained After Unidirectional Freezing and Ice-Segregation-Induced Self-Assembly," Chem. Mater., **20**(3), pp. 634–648.
[15] Nishihara, H., Mukai, S. R., Yamashita, D., and Tamon, H., 2005, "Ordered Macroporous Silica by Ice Templating," Chem. Mater., **17**(3), pp. 683–689.
[16] Song, X., Tetik, H., Jirakittsonthon, T., Parandoush, P., Yang, G., Lee, D., Ryu, S., Lei, S., Weiss, M. L., and Lin, D., 2019, "Biomimetic 3D Printing of Hierarchical and Interconnected Porous Hydroxyapatite Structures With High Mechanical Strength for Bone Cell Culture," Adv. Eng. Mater., **21**(1), p. 1800678.
[17] Bozkurt, A., Brook, G. A., Moellers, S., Lassner, F., Sellhaus, B., Weis, J., Woeltje, M., Tank, J., Beckmann, C., Fuchs, P., Damink, L. O., Schügner, F., Heschel, I., and Pallua, N., 2007, "In Vitro Assessment of Axonal Growth Using Dorsal Root Ganglia Explants in a Novel Three-Dimensional Collagen Matrix," Tissue Eng., **13**(12), pp. 2971–2979.
[18] Qi, X., Ye, J., and Wang, Y., 2009, "Alginate/Poly, Lactic-co-Glycolic Acid)/Calcium Phosphate Cement Scaffold With Oriented Pore Structure for Bone Tissue Engineering," J. Biomed. Mater. Res. Part A, **89**(4), pp. 980–987.
[19] Kaczmarek-Pawelska, A., 2020, "*Alginate-Based Hydrogels in Regenerative Medicine*," Alginates—Recent Uses of This Natural Polymer, IntechOpen, Rijeka, Croatia.
[20] GhavamiNejad, A., Ashammakhi, N., Wu, X. Y., and Khademhosseini, A., 2020, "Crosslinking Strategies for 3D Bioprinting of Polymeric Hydrogels," Small, **16**(35), p. 2002931.
[21] Yang, L., Tanabe, K., Miura, T., Yoshinari, M., Takemoto, S., Shintani, S., and Kasahara, M., 2017, "Influence of Lyophilization Factors and Gelatin Concentration on Pore Structures of Atelocollagen/Gelatin Sponge Biomaterial," Dental Mater. J., **36**(4), pp. 429–437.
[22] Shahbazi, M. A., Ghalkhani, M., and Maleki, H., 2020, "Directional Freeze-Casting: A Bioinspired Method to Assemble Multifunctional Aligned Porous Structures for Advanced Applications," Adv. Eng. Mater., **22**(7), p. 2000033.
[23] Annabi, N., Nichol, J. W., Zhong, X., Ji, C., Koshy, S., Khademhosseini, A., and Dehghani, F., 2010, "Controlling the Porosity and Microarchitecture of Hydrogels for Tissue Engineering," Tissue Eng. Part B Rev., **16**(4), pp. 371–383.
[24] Kim, G., Ahn, S., Yoon, H., Kim, Y., and Chun, W., 2009, "A Cryogenic Direct-Plotting System for Fabrication of 3D Collagen Scaffolds for Tissue Engineering," J. Mater. Chem., **19**(46), pp. 8817–8823.
[25] Liu, H., Zhang, G., and Li, H., 2017, "Preparation and Properties of GO-PVA Composite Hydrogel With Oriented Structure," AIP Conf. Proc., **1820**(1), p. 030009.
[26] Fu, S., Thacker, A., Sperger, D. M., Boni, R. L., Buckner, I. S., Velankar, S., Munson, E. J., and Block, L. H., 2011, "Relevance of Rheological Properties of Sodium Alginate in Solution to Calcium Alginate Gel Properties," AAPS PharmSciTech, **12**(2), pp. 453–460.
[27] Sahoo, D. R., and Biswal, T., 2021, "Alginate and Its Application to Tissue Engineering," SN Appl. Sci., **3**(1), pp. 1–19.
[28] Kuo, C. K., and Ma, P. X., 2008, "Maintaining Dimensions and Mechanical Properties of Ionically Crosslinked Alginate Hydrogel Scaffolds in Vitro," J. Biomed. Mater. Res. Part A, **84**(4), pp. 899–907.
[29] Hurler, J., Engesland, A., Poorahmary Kermany, B., and Škalko-Basnet, N., 2012, "Improved Texture Analysis for Hydrogel Characterization: Gel Cohesiveness, Adhesiveness, and Hardness," J. Appl. Polym. Sci., **125**(1), pp. 180–188.